Tight-binding calculation of the optical absorption cross section of spherical and ellipsoidal silicon nanocrystals

F. Trani,* G. Cantele, D. Ninno, and G. Iadonisi
Coherentia CNR-INFM and Università di Napoli "Federico II"—Dipartimento di Scienze Fisiche
Complesso Universitario Monte S. Angelo, Via Cintia, I-80126 Napoli, Italy
(Received 28 July 2004; revised manuscript received 2 May 2005; published 15 August 2005)

Electronic and optical properties of silicon nanocrystals are calculated and discussed within a semiempirical tight-binding approach, which allows to study systems composed of thousands of atoms. Oscillator strengths, frequency-dependent optical absorption cross sections, and static dielectric constants are investigated for both spherical and ellipsoidal nanocrystals, with the aim of pointing out their size- and shape-dependent features. We show that the anisotropy of the optical functions follows the nanocrystal shape, and a comparison is discussed between very elongated structures and quantum wires.

DOI: 10.1103/PhysRevB.72.075423 PACS number(s): 78.67.Bf, 78.20.Ci, 31.15.Ct, 73.22.Dj

I. INTRODUCTION

Great interest has been devoted in the last years to the study of the optical properties of silicon nanocrystals and porous silicon. Despite the large amount of papers that have been published on this subject, there still are some aspects which are controversial and not fully understood. Just to give a few examples, we can mention the Stokes shift between the absorption gap and the photoluminescence peak,[1–3] the annihilation of the oscillator strengths,[4,5] the origin of the photoluminescence, the role of excitons and surface states.[6–9]

From the theoretical point of view, there are many approaches which allow the investigation of the optical and electronic properties of nanostructured materials. *Ab initio* methods[10–13] have been widely used, due to the possibility of giving a fully atomistic description of these systems. They have become very efficient thanks to the continuous increasing of both computer performance and algorithm speed. Nevertheless, semiempirical methods remain a powerful tool,[14,15] giving the chance to simulate real nanocrystals, made of tens of thousands of atoms, with diameters of several nanometers. The properties of large nanocrystals are both quantitatively and qualitatively described within such approaches, provided that the transferability of the parameters from the bulk to the nanoscale is an acceptable approximation. In this paper we consider a semiempirical tight-binding (TB) method,[16] based on a set of localized wave functions, that is very efficient in the study of large structures. The determination of the electronic spectrum is reduced to the diagonalization of a reasonable matrix, having the dimension of a few times the number of atoms, and a very high degree of sparsity. Taking advantage of both the matrix sparsity and the symmetry of the structure under study, one can have a significant reduction of the computational load. However, most of the semiempirical TB methods do not generally allow an explicit calculation of the nanocrystal wave functions, and a suitable approximation for the momentum matrix elements between atomic orbitals is needed for optical properties calculations.[17–21]

Using a TB approach, which will be described in the next section (Sec. II), we have performed a detailed analysis of size- and shape-dependent features of the electronic spectra and absorption cross section of silicon nanocrystals. First, quantum confinement effects are investigated for spherical structures with different size (Sec. III). We show results concerning the optical absorption cross section and the oscillator strength, and compare them with previous calculations. Next, the dependence of such properties on the nanocrystal shape will be addressed (Sec. IV). Recently, we have studied the infrared optical properties of ellipsoidal silicon nanocrystals, calculating the electronic states within both the effective mass theory[22–24] and the TB formalism.[25,26] Here, we extend this study to across-gap transitions motivated by the fact that the dielectric function for ellipsoidal structures has not been widely investigated, and a systematic study is still lacking. The effects of moderate deviations from the spherical shape on the energy levels and on the photoluminescence properties have been studied within the framework of the effective mass approximation.[27] These studies have been performed especially for direct gap semiconductors, such as the II–VI nanocrystals.[28] For silicon nanocrystals the subject has been discussed in a recent paper,[29] where the question of the luminescence polarization in elongated silicon nanocrystals is addressed and a comprehensive study of the optical transition rates is made within a TB scheme. However, the authors have considered nanostructures with a limited number of aspect ratios and, more importantly, have not studied the absorption cross section, which is an experimentally accessible quantity. In this paper we shall attempt to fill this important gap for both the spherical and ellipsoidal silicon nanocrystals, underlining, for the latter ones, the interplay between the nanocrystal shape and the absorption spectrum asymmetry.

It is worth mentioning that recent papers[30–32] have shown the possibility of forming porous silicon samples whose nanostructures are mainly made of anisotropic nanocrystallites. The photoluminescence from these samples is characterized by a significant polarization anisotropy which has been interpreted within a dielectric model made of ellipsoidal structures, with a given static isotropic dielectric constant, embedded in an effective medium. Polarization anisotropy related to across-gap transitions has not been considered and will be discussed in the following sections.

 ©2005 The American Physical Society

Moreover, very recently, polarized optical gain has been obtained from a porous silicon layer.[33] It is likely that ultrasmall elongated silicon nanostructures are responsible for this phenomenon.

II. THE TIGHT-BINDING METHOD

We use an sp^3 TB model with inclusion of three center integrals, and interactions up to the third-nearest neighbors. This model is based on a set of 20 independent parameters, fitted to obtain a reasonable band structure and good values of the main band gaps and effective masses.[15] These parameters allow the calculation of the density of states and of the electronic spectra of silicon structures. The optical dielectric function within the random-phase approximation (RPA) can be written as

$$\epsilon^{\alpha\beta}(E) = \delta_{\alpha,\beta} + \frac{4\pi e^2\hbar^2}{m\Omega}\sum_{n,n'}(\eta_{n'} - \eta_n)\frac{F^{\alpha\beta}_{n,n'}}{E_{n,n'}}\left[\frac{1}{E - E_{n,n'} + i\gamma}\right], \tag{1}$$

where $\Omega = N_{Si}a^3/8$ is the structure volume (N_{Si} is the number of silicon atoms, and a is the bulk silicon lattice constant),[15,34] m is the free-electron mass, η_n is the occupation number for the nth nanocrystal state, $E_{n,n'}$ and $F^{\alpha\beta}_{n,n'}$ are, respectively, the transition energy and the α,β component of the oscillator strength associated with the $|n\rangle \rightarrow |n'\rangle$ transition; a factor of 2 takes into account the spin degeneracy and the sum is done over all the states. In our calculations local field and excitonic effects are neglected and a Lorentzian shape is used for the broadening. The oscillator strength is defined by

$$F^{\alpha\beta}_{n,n'} = \frac{2\langle n|\hat{p}_\alpha|n'\rangle\langle n'|\hat{p}_\beta|n\rangle}{mE_{n,n'}}, \tag{2}$$

where the matrix elements between the nanocrystal states are given by

$$\langle n|\hat{p}_\alpha|n'\rangle = \sum_{\mathbf{R},\mathbf{R}',\sigma,\sigma'} B_{\sigma,n}(\mathbf{R})\langle \mathbf{R},\sigma|\hat{p}_\alpha|\mathbf{R}',\sigma'\rangle B_{\sigma',n'}(\mathbf{R}'). \tag{3}$$

In this equation, $\mathbf{R}$ is the position of an atom in the structure, σ labels the symmetry of the atomic orbital $|\mathbf{R},\sigma\rangle$, $B_{\sigma,n}(\mathbf{R})$ are the eigenvectors coming from the diagonalization of the TB Hamiltonian, and the sum is done all over the silicon atoms contained in the structure. The corresponding equations for a bulk periodic crystal are easy to write. In both cases, it is necessary to have an evaluation of the momentum matrix elements between the atomic orbitals which, in an empirical TB scheme, are not explicitly known. A procedure, developed in Ref. 35, has raised new interest in recent years, and many researchers have been trying to deduce it from a very general point of view.[20,36–38] Starting from the parametrization of the position operator matrix elements, the momentum elements are calculated by making use of both the almost completeness of the TB basis set and the operator identity[19,35]

$$\hat{\mathbf{p}} = \frac{m}{i\hbar}[\hat{\mathbf{r}}, \hat{H}]. \tag{4}$$

Because of the translational symmetry, the bulk Si position matrix elements in an orthogonal TB basis set can be written as

$$\langle \mathbf{R},\sigma|\hat{\mathbf{r}}|\mathbf{R}',\sigma'\rangle = \mathbf{R}\delta_{\mathbf{R},\mathbf{R}'}\delta_{\sigma,\sigma'} + [\mathbf{D}(\mathbf{R}-\mathbf{R}')]_{\sigma,\sigma'}, \tag{5}$$

where

$$[\mathbf{D}(\mathbf{R})]_{\sigma,\sigma'} = \langle \mathbf{0},\sigma|\hat{\mathbf{r}}|\mathbf{R},\sigma'\rangle. \tag{6}$$

The approximation that we use consists of retaining only the diagonal term in Eq. (5), therefore treating the TB atomic orbitals as eigenstates of the position operator. By using this approximation, the momentum matrix elements in the TB basis set are written as

$$\mathbf{P}(\mathbf{R},\mathbf{R}') = \frac{m}{i\hbar}[\mathbf{R}-\mathbf{R}']H(\mathbf{R},\mathbf{R}'). \tag{7}$$

Here, $H(\mathbf{R},\mathbf{R}')$ is the Hamiltonian matrix. From Eq. (7) it is seen that $\mathbf{P}$ depends only on the Hamiltonian matrix; it is very simple to evaluate, no additional parameters being requested in the calculation (the Hamiltonian matrix is fully determined from the bulk band structure fitting). This approach satisfies the gauge invariance and the $\mathbf{q}\rightarrow\mathbf{0}$ limit of the charge-conserving equation.[20,38] This is an important check of self-consistency that every model should satisfy, in order to have equality between density and current response.[17] There has been a recent discussion in the literature on whether the further on-site position matrix elements should be added in Eq. (5).[37–40] These terms are related to the atomic polarizability. Since we expect, on physical grounds, that an atom in a bulk semiconductor crystal is less polarizable than the bonds with its neighbors, we neglect these contributions, retaining only the first term in Eq. (5). It is difficult to give an estimation of the error induced by this approximation because it may strongly depend on the TB parametrization used, and also because it could break the gauge invariance.[37,38] Nevertheless, for addressing the quality of both the TB parametrization and the approximation in Eq. (7), we have calculated the imaginary part of the optical dielectric function for bulk silicon and compared it with both the experimental data and those obtained from an empirical pseudopotential calculation. In this last case we have used the pseudopotential form factors of Ref. 41 with a standard Monkhorst-Pack procedure for the integration in the first Brillouin zone. The results are shown in Fig. 1, where the TB curves are calculated with the parameters of Refs. 15 and 16, and the experimental data are taken from Ref. 42. It can be seen from this figure that there is a satisfactory agreement between the three calculated curves and the experimental data, with the exception of the peak around ~3.4 eV, which is related to the formation of excitons[43] which are not considered in this work. As a check, following Refs. 19 and 40, we have also added just one intra-atomic dipole matrix element through Eq. (6), setting $\mathbf{D}(\mathbf{R}-\mathbf{R}') = \mathbf{d}_{sp_x}\delta_{\mathbf{R}-\mathbf{R}'}$ with $\mathbf{d}_{sp_x} = 0.027$ nm. We have found that this addition introduces only minor numerical changes to the TB curves of Fig. 1.

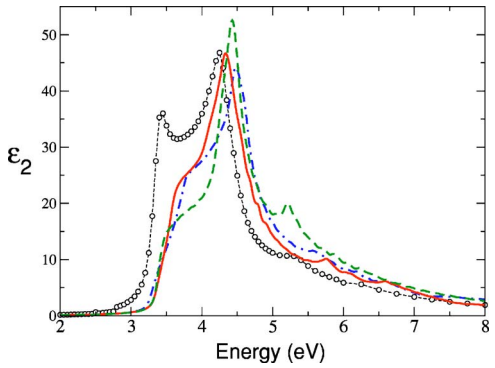

FIG. 1. (Color online) Imaginary part of the bulk silicon dielectric function. The empty circles are experimental data (Ref. 42); the solid and the dot-dashed lines are the TB curves calculated using, respectively, Tserbak (Ref. 16) and Niquet (Ref. 15) parameters; the dashed line refers to a local empirical pseudopotential calculation performed with the Chelikowsky-Cohen (Ref. 41) form factors.

This insensitivity is surely due to the TB parametrization we are using, which includes interactions up to the third-nearest neighbors, whereas those used in Refs. 19 and 40 is an sp^3s^* with only first neighbors.

The static dielectric constant can be obtained as

$$\epsilon_s = 1 + \frac{2}{\pi}\int_0^\infty \frac{\epsilon_2(E)}{E}dE. \tag{8}$$

From our TB curves we get 10.63 and 10.74 using Tserbak[16] and Niquet[15] parameters, respectively. These values are comparable with the experimental result[44] of 11.4 and with the local empirical pseudopotential result of 10.3 (a 10% error is usually ascribed to exciton effects). As a final check, we have calculated the "f-sum rule" for the imaginary part of the dielectric function

$$\frac{m\Omega}{2N\pi^2e^2\hbar^2}\int_0^\infty E\epsilon_2(E)dE = 1, \tag{9}$$

where N is the number of electrons contained inside the volume Ω. In the case of bulk silicon, we obtain the value of 1.077 with both sets of TB parameters so that the sum rule is satisfied to within 10%. The calculations for both the spherical and ellipsoidal nanostructures we are going to discuss in the following sections are all based on the TB parameters of Ref. 15.

An optical function closely related to the imaginary part of the dielectric function is the absorption cross section, which we define as[45]

$$\sigma(E) = 2\frac{\sigma_e}{4N_{Si}}\sum_{n,n'}\eta_n(1-\eta_{n'})F_{nn'}S(E-E_{nn'}). \tag{10}$$

Here, we have used $S(E)$ for indicating the broadening of the energy levels; a factor of 2 takes into account the spin degeneracy, while $\sigma_e = 2\pi^2\hbar e^2/mc \simeq 1.098$ eV Å^2 is the complete one-electron oscillator strength. In our calculations, we assume that the nanocrystal is embedded in a dielectric medium with a refraction index of 1, and we neglect local field effects. The choice of calculating the absorption cross section concerns both the fact that it is experimentally accessible[6,46] and useful for evaluating the absorption gap energy.[5,47,48] Indeed, the onset of the optical absorption can be defined by requiring that the integration up to this energy of the absorption cross section is a certain fraction p of the complete one-electron oscillator strength σ_e. We have used a threshold parameter $p = 10^{-4}$, which is fully consistent with the very recent measurements of oscillator strengths.[49]

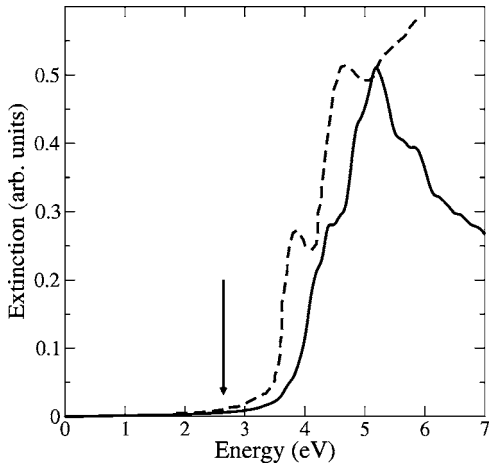

FIG. 2. Extinction coefficient for a Si nanocrystal having the diameter of about 1.8 nm, obtained from absorption measurements (Ref. 50) (dashed line), compared to the $Si_{159}H_{124}$ (d=1.83 nm) extinction coefficient, calculated within our TB method (solid line). The arrow labels the first calculated transition energy. Our theoretical data have been rescaled in such a way that the two curves have the same height of the main peak.

III. SPHERICAL NANOCRYSTALS

In this section we investigate the optical properties of spherical silicon nanocrystals with all the surface dangling bonds saturated by hydrogen, with the aim of pointing out their size-dependent features. Dipole-allowed transition energies, as a function of the nanocrystal diameter, have already been reported in Ref. 15, and the comparison with the experimental data is discussed in Ref. 2. Since we use exactly the same TB parametrization, we will not reproduce those results here.

Using the method described in the previous section, we have calculated the nanocrystal absorption cross section. As a further check of the method, we have compared the calculated extinction coefficient of the $Si_{159}H_{124}$ nanocrystal (which has an equivalent diameter of 1.83 nm) to the experimental curve given by Wilcoxon *et al.*[50] for a silicon nanocrystal with an estimated diameter of about 1.8 nm. The two curves are shown in Fig. 2, where the arrow indicates the first calculated dipole-allowed transition energy. We have rescaled our theoretical data in such a way that the two curves have the same height at the main peak. We want to point out the great similarity of the two curves. In fact, although an overestimation of the calculated dielectric function is intrinsic to the parametrization we use, as it was already

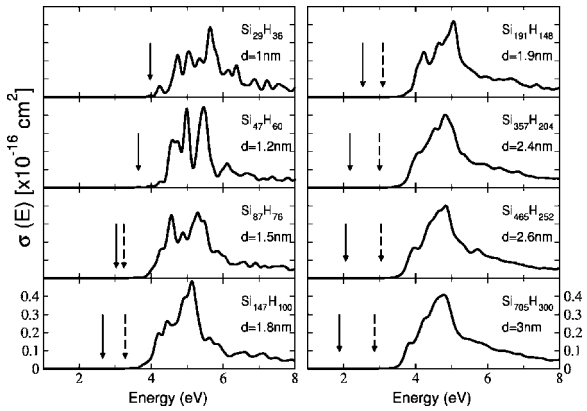

FIG. 3. Absorption cross section for a set of spherical nanocrystals. A 0.1 eV Gaussian broadening has been used. The solid arrows show the first dipole-allowed transition (HOMO-LUMO gap); the dashed arrows point to the absorption gap, as defined in the text. For the first two structures, the first allowed transition and the absorption gap have the same value. Calculations have been performed for structures with increasing diameter.

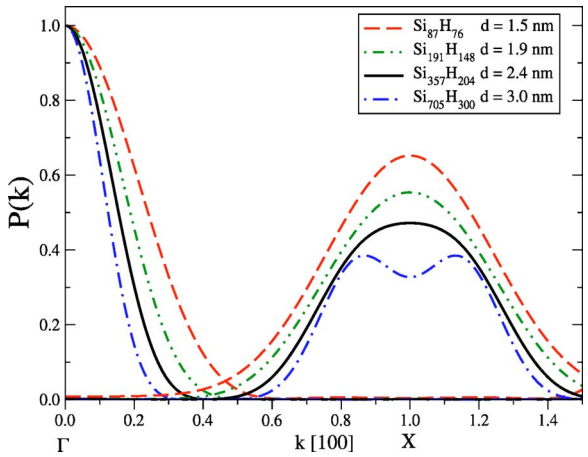

FIG. 4. (Color online) *k*-space projection of the spherical nanocrystals eigenstates on the bulk Si band complex. The curves centered on Γ and *X* are, respectively, the projections of the HOMO and LUMO nanocrystal states. The normalization has been done in such a way that the HOMO states projection is 1 at Γ.

clear for the bulk in Fig. 1, a fair agreement in the relative positions and intensities of the two main peaks emerges from Fig. 2.

The absorption cross section for a set of nanocrystals with increasing size is shown in Fig. 3. In this figure the full arrows mark the energy of the first dipole-allowed transition, which, for our structures, coincides with the HOMO-LUMO gap, defined as the difference between the lowest unoccupied state (LUMO) and the highest occupied state (HOMO) energy, while the dashed arrows indicate the energy of the optical absorption threshold calculated with the criteria described at the end of the previous section. An interesting result is that, for small structures, the two onsets are basically coincident while, upon increasing the dimension, the optical absorption gap approaches the bulk Γ–Γ gap while the HOMO-LUMO gap goes to the bulk Γ–*X* indirect gap. Extensive calculations on clusters even larger than those showed in Fig. 3 have confirmed this trend, with the optical functions progressively matching those of bulk silicon. For a deeper understanding of this trend, we have calculated the projections of the nanocrystal wave functions on the first bulk Brillouin zone. This is motivated by the fact that the transition rates are basically proportional to the *k*-space overlap between the HOMO and LUMO wave functions. In Fig. 4 we report the Δ line projection of the nanocrystal states (the sum is done on all the quasidegenerate energy levels) on the bulk Si band complex subspace constituted by the upper valence bands and the lower conduction bands included in our TB calculation. It emerges from this figure that, while HOMO states are localized around Γ, the LUMO takes components mainly around the six *X* valleys. It is worth noting that, upon increasing the nanocrystal diameter, the overlap between HOMO and LUMO states annihilate very quickly. Moreover, the LUMO projection is well centered on *X* when the nanocrystal size is smaller than a certain threshold. For diameters higher than this threshold, the maximum of the LUMO states goes away from *X*, tending to the bulk limit of about 0.83. This behavior leads to a fast annihilation of the oscillator strengths upon increasing the nanocrystal size. Therefore, although for a nanocrystal all the transitions are direct, the indirect nature of the starting bulk material is still there. We think that this behavior, characteristic of indirect semiconductors, is at the basis of the difficulties of a correct understanding of the silicon nanostructures photoluminescence phenomena.[6]

In order to be more quantitative, we show in Fig. 5 the lowest-energy oscillator strengths and the electron-hole radiative recombination time versus the transition energies for a set of spherical nanocrystals. It is clearly seen that, even for very small crystallites, the dipole-allowed transitions have oscillator strengths of the order of magnitude of 10^{-1}, tending to annihilate rapidly as the nanocrystal size increases. The point here is that, going from the HOMO-LUMO gap to

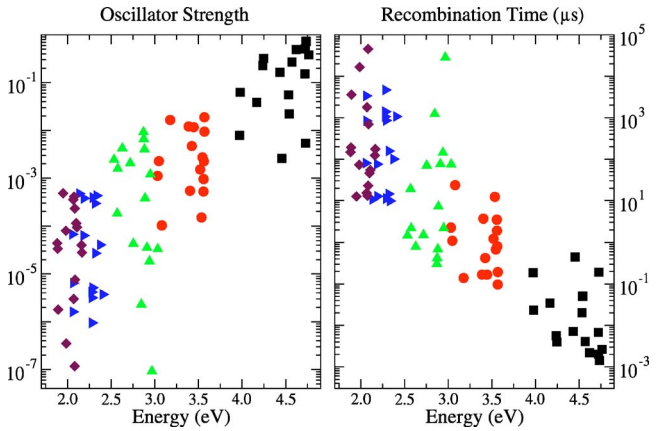

FIG. 5. (Color online) Oscillator strengths (left) and electron-hole radiative recombination times (right) for the lowest-energy transitions, calculated for a set of spherical silicon nanocrystals. The results shown in figure refer to the following nanocrystals: $Si_{29}H_{36}$ (d=1 nm), squares; $Si_{87}H_{76}$ (d=1.5 nm), circles; $Si_{191}H_{148}$ (d=1.9 nm), triangles-up; $Si_{465}H_{252}$ (d=2.6 nm), triangles-right; $Si_{705}H_{300}$ (d=3 nm), diamonds.

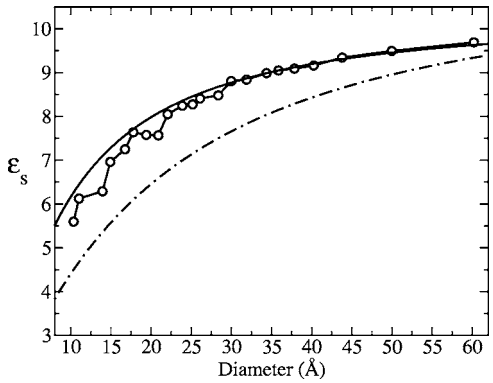

FIG. 6. Calculated spherical nanocrystal static dielectric constant. The circles correspond to our TB results (the line is only a guide for the eyes). The solid line is the pseudopotential result from Ref. 34, while the dot-dashed line is the TB calculation of the screening average dielectric constant of Ref. 54. The data from Ref. 34 have been taken without any rescaling (see the text).

well above the optical absorption gap, there is a large number of transitions with relatively small oscillator strengths reflecting the intrinsic indirect nature of silicon mentioned above. This finding is consistent with the theoretical work of Ref. 4. Moreover, it seems that both the trend and the order of magnitude of our calculated oscillator strengths are in a good agreement with the recent experimental measurements of Ref. 49. Instead, upon increasing the nanocrystal size, the radiative recombination times increase. We found that, for a 3 nm nanocrystal (with energies at about 2 eV), the recombination time is already $\tau_{rad} \simeq 10\ \mu$s. When the nanocrystals size changes from a few angstrom to several nanometers, the radiative recombination times change from the range of the nanosecond ($d \simeq 1$ nm) to the microsecond ($d \simeq 3$ nm) to the millisecond (bulk Si). For large-size nanocrystals, the electron-phonon contribution should be added into the calculation.[51,52] The general trend of our results is in agreement with previous findings in the literature.[12,53]

Finally, we have calculated the static dielectric constant ϵ_s using Eq. (8). The results are shown in Fig. 6, together with both the empirical pseudopotentials results of Wang *et al.*[34] and the self-consistent TB results of Allan *et al.*[54] It should be noted that Wang *et al.*[34] have rescaled their data in such a way to reproduce the measured bulk silicon static dielectric constant. We preferred to avoid such a rescaling so that, in order to have a consistent comparison with our results, we have rescaled back their data. The good agreement between our results and those of Ref. 34 is expected simply because in both cases ϵ_s is calculated from Eq. (8). The TB result of Ref. 54 is reported here for completeness and lies lower, being the average screening dielectric constant of a hydrogenic impurity.

Although the calculated dielectric constant shows a small scatter due to the molecular structure of the nanocrystals,[54] we can safely confirm that it is an increasing function of the nanocrystal size.

IV. ELLIPSOIDAL NANOCRYSTALS

Shape-dependent features of the dielectric and optical properties can be obtained applying the TB approach to ellipsoidal nanocrystals. The nanocrystals are built starting from a central silicon atom, and including all the atoms (at the bulk positions) lying inside the surface

$$\frac{x^2+y^2}{a^2}+\frac{z^2}{c^2}=1, \tag{11}$$

where the z axis has been taken along the [001] direction, and all the surface silicon atoms have been saturated by hydrogen. We define $\chi=c/a$ as the ellipsoid aspect ratio. In Ref. 25, where some computational details may be found, we already analyzed the LUMO states and the corresponding infrared transition energies. Moreover, some preliminary results on the optical dielectric tensor have been presented in Ref. 26. Here, we focus on the across-gap optical properties and the degree of linear polarization, showing how they depend on the geometrical anisotropy. The static dielectric tensor of silicon ellipsoidal nanocrystals is calculated and discussed. Finally, we consider the limit of elongated ellipsoidal quantum dots, comparing the calculated absorption cross section with that of a quantum wire. It is worth pointing out that anisotropy-dependent optical properties are closely related to the recent measurements of birefringence in optical waveguides made on silicon nanocrystal superlattices,[55] and can be at the basis of a theoretical explanation of the polarized optical gain found in porous silicon layers.[33]

Shape-related aspects due to quantum confinement in anisotropic structures are investigated considering a set of ellipsoidal nanocrystals all having the same a semiaxis in the $x-y$ plane but different values of the aspect ratio χ. Within this set, a wide range of geometries is considered, retrieving a disklike structure or a cylindrical quantum wire in the limits $\chi \to 0$ and $\chi \to \infty$, respectively.

Because of the rotational symmetry (all the ellipsoids are built in such a way to have D_{2d} symmetry[56]), we have two possible polarizations for the ellipsoid optical transitions: the perpendicular polarization whose vectors lie in the plane orthogonal to the ellipsoid symmetry axis, and the parallel polarization, whose vectors lie along the c direction. Figure 7 shows the independent components of the absorption cross section for a set of ellipsoids with $a=1$ nm and with the aspect ratio ranging from $\chi=0.5$ to $\chi=3$. We also show, for each ellipsoid, the first dipole-allowed transition energy (dotted arrow), which we find to be insensitive to the transition polarization, and the absorption gap calculated as in the previous section for both the perpendicular (solid arrow) and the parallel (dashed arrow) polarization. We point out the interesting result that, contrary to the first transition energy, the absorption gap depends on the polarization. The anisotropic effects are especially pronounced in the oblate case ($\chi<1$). Instead, in the limit of large, prolate ($\chi>1$) nanocrystals, the difference between the two curves becomes quite small. At the same time, the first dipole-allowed transition goes far away from the absorption threshold. In the limit of a very elongated structure, we retrieve the quantum wire absorption spectrum. In order to check this point, we have calculated, in an independent way, the absorption cross section of a [001] quantum wire having a circular section radius $r=1$ nm. The comparison between the ellipsoid with $\chi=3$ and the quantum

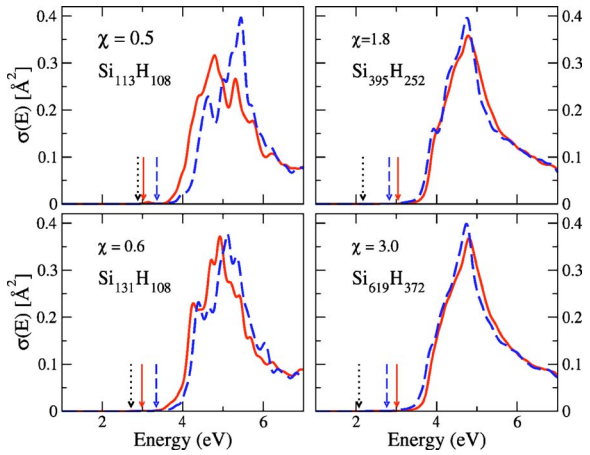

FIG. 7. (Color online) Absorption cross section for a set of Si ellipsoids with $a=1$ nm, as a function of the aspect ratio χ. The solid and the dashed curves refer, respectively, to the perpendicular and the parallel polarization. The dotted arrow is the first transition energy, which is almost insensitive to the polarization. The solid and dashed arrows point, respectively, to the perpendicular and parallel absorption thresholds. A 0.1 eV Gaussian broadening has been used.

wire limit is shown in Fig. 8 for both the perpendicular (upper figure) and the parallel (lower figure) polarization. From Fig. 8 emerges an overall agreement between the ellipsoid and wire results. This is not surprising, in that the number of Si atoms along the z direction is huge, and so we expect that the quantum confinement has a non-negligible effect only along the other directions. Nevertheless, we note here the presence of an energy gap between the onsets of the two structures, due to a slow convergence of the ellipsoid transition energies to the quantum wire limit.[57] Finally, it is worth remarking that our results are consistent with other calcula-

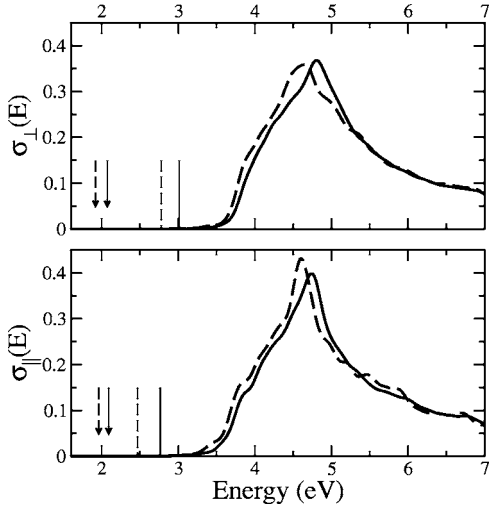

FIG. 8. Comparison between an ellipsoid with $a=1$ nm, $\chi=3$ (dashed lines), and a [001] cylindrical quantum wire having a radius $r=1$ nm (solid lines). The absorption cross section is shown for both the perpendicular (upper panel) and the parallel (lower panel) polarization. The arrows point to the first dipole-allowed transition, whereas the lines point to the absorption threshold.

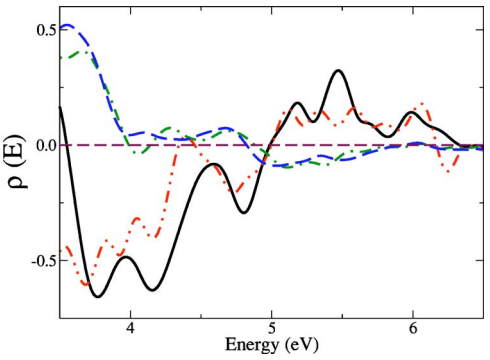

FIG. 9. (Color online) Degree of linear polarization ρ for the ellipsoid frequency-dependent absorption cross section, defined in Eq. (12), plotted for $a=1$ nm and different values of the aspect ratio: $\chi=0.5$, solid line; $\chi=0.6$, double dot-dashed line; $\chi=1.8$, dot-dashed line; $\chi=3.0$, dashed line.

tions. Indeed, our dielectric function can be compared to previous quantum wire results.[21,58,59]

It is useful to give a quantitative estimation of the optical anisotropy effects by introducing the degree of linear polarization for the absorption cross section (according to the usual definition given for the photoluminescence intensity[29,30]), defined as

$$\rho = \frac{\sigma_{\parallel} - \sigma_{\perp}}{\sigma_{\parallel} + \sigma_{\perp}}. \tag{12}$$

In Fig. 9 we show ρ, obtained from the data of Fig. 7, as a function of the energy. An interesting feature is that, for each nanocrystal, a sign inversion of ρ appears at a fixed energy of about 5 eV. For this energy the cross section is independent of the polarization. A symmetry change comes out in correspondence with the geometrical shape change from oblate to prolate structures. For energies lower than 5 eV, the degree of linear polarization σ is negative for oblate structures and positive for the prolate ones. This means that, in the range of energies below 5 eV, oblate silicon ellipsoids mainly absorb an $x-y$ polarized radiation, while prolate nanocrystals mainly absorb a z-polarized radiation. It is worth pointing out again that within this analysis we do not take into account depolarization factors and local field effects, which may be important for porous silicon.[31]

The static dielectric constant can be obtained from the optical dielectric function using Eq. (8). In this case the two different components $\epsilon_{s\perp}$ and $\epsilon_{s\parallel}$ have to be considered, and are shown in Fig. 10 (left panel) as a function of χ. The crossing between the two components occurring at $\chi=1$ (spherical nanocrystal) is due to the change of the structure from oblate to prolate. Also, in this case we can define a degree of linear polarization ρ_s with a formula similar to Eq. (12). The results are shown in Fig. 10 (right panel), where ρ_s has been calculated as a function of χ. From this figure we notice an interesting correlation between the nanocrystal shape and the dominant component of the static dielectric constant. For oblate structures the perpendicular component is larger, while for the prolate ones the parallel component is larger.

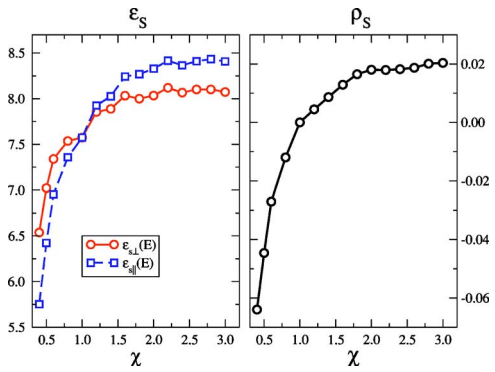

FIG. 10. (Color online) Left panel: Principal components of the static dielectric tensor for a set of ellipsoids with a fixed semiaxis $a=1$ nm. The circles and the squares are, respectively, the perpendicular and the parallel component with respect to the nanocrystal symmetry axis. Right panel: The static dielectric tensor degree of linear polarization. The lines are guides for the eyes.

V. CONCLUSIONS

We have used a TB approach for the study of size- and shape-dependent features of the optical properties of silicon nanocrystals. Single-particle energy spectra, dipole-allowed transition energies, oscillator strengths and radiative lifetimes, absorption cross section, and static dielectric constant have been calculated for both spherical and ellipsoidal silicon nanocrystals. The results for both the spherical and ellipsoidal structures show a significant annihilation of the oscillator strengths with the nanocrystal size. At the same time, the HOMO-LUMO gap and the optical absorption gap become different for large structures and, in the case of a spherical shape, the limit values are the indirect and direct bulk silicon gap, respectively. We have also found that very elongated nanocrystals show the limit behavior of the quantum wire. It is expected that very flattened structures have a quantum disk as a limit.

The optical dielectric function has been calculated from the dipole matrix elements without the addition of on-site terms. The good agreement with the measured bulk ϵ_2 is an indication that the neglected terms would have very little numerical significance on the calculated curves. Assuming the transferability of the dipole matrix elements from the bulk to the confined structure (this is a prerequisite of any semiempirical method), we have calculated the optical absorption cross section for both spherical and ellipsoidal structures. Our calculations are consistent with previous empirical-pseudopotential results on spherical nanocrystals. More interestingly, the absorption cross section of ellipsoidal nanocrystals is shown to have an anisotropy which follows the nanocrystal shape. The same behavior has also been found for the static dielectric constant.

We believe that these results can help in a full understanding of some aspects related to quantum confinement in porous silicon samples. In fact, models based on ensemble of silicon ellipsoids have been shown to give a good agreement with the photoluminescence data.[30–32] Moreover, this study can help in understanding the polarized optical gain recently obtained from a porous silicon layer.[33] In addition, recent experiments have demonstrated the possibility of fabricating well-passivated, small-diameter silicon nanowires.[60] It is not difficult to think that, in a few years, silicon nanorods and ellipsoids will be available as well.

ACKNOWLEDGMENTS

Financial support from the ENEA project POSSENTE and from the MIUR-PON project SVISENARIA is acknowledged.

*Electronic address: fabio.trani@na.infn.it

[1] D. J. Lockwood, Solid State Commun. **92**, 101 (1994).
[2] C. Delerue, G. Allan, and M. Lannoo, J. Lumin. **80**, 65 (1999).
[3] E. Degoli, G. Cantele, E. Luppi, R. Magri, D. Ninno, O. Bisi, and S. Ossicini, Phys. Rev. B **69**, 155411 (2004).
[4] B. Delley and E. F. Steigmeier, Phys. Rev. B **47**, 1397 (1993).
[5] I. Vasiliev, S. Öğüt, and J. R. Chelikowsky, Phys. Rev. Lett. **86**, 1813 (2001).
[6] D. Kovalev, H. Heckler, G. Polisski, and F. Koch, Phys. Status Solidi B **215**, 871 (1999).
[7] F. A. Reboredo, A. Franceschetti, and A. Zunger, Phys. Rev. B **61**, 13073 (2000).
[8] M. V. Wolkin, J. Jorne, P. M. Fauchet, G. Allan, and C. Delerue, Phys. Rev. Lett. **82**, 197 (1999).
[9] C. Delerue, M. Lannoo, and G. Allan, Phys. Status Solidi B **227**, 115 (2001).
[10] I. Vasiliev, S. Öğüt, and J. R. Chelikowsky, Phys. Rev. B **65**, 115416 (2001).
[11] L. X. Benedict, A. Puzder, A. J. Williamson, J. C. Grossman, G. Galli, J. E. Klepeis, J. Y. Raty, and O. Pankratov, Phys. Rev. B **68**, 085310 (2003).
[12] H.-C. Weissker, J. Furthmüller, and F. Bechstedt, Phys. Rev. B **69**, 115310 (2004).
[13] C. S. Garoufalis, A. D. Zdetsis, and S. Grimme, Phys. Rev. Lett. **87**, 276402 (2001).
[14] L. W. Wang and A. Zunger, J. Phys. Chem. **98**, 2158 (1994).
[15] Y. M. Niquet, C. Delerue, G. Allan, and M. Lannoo, Phys. Rev. B **62**, 5109 (2000).
[16] C. Tserbak, H. M. Polatoglou, and G. Theodorou, Phys. Rev. B **47**, 7104 (1993).
[17] W. Hanke and L. J. Sham, Phys. Rev. B **21**, 4656 (1980).
[18] J. Petit, G. Allan, and M. Lannoo, Phys. Rev. B **33**, 8595 (1986).
[19] A. Selloni, P. Marsella, and R. DelSole, Phys. Rev. B **33**, 8885 (1986).
[20] M. Graf and P. Vogl, Phys. Rev. B **51**, 4940 (1995).
[21] G. D. Sanders and Y.-C. Chang, Phys. Rev. B **45**, 9202 (1992).
[22] G. Cantele, D. Ninno, and G. Iadonisi, J. Phys.: Condens. Matter **12**, 9019 (2000).
[23] G. Cantele, G. Piacente, D. Ninno, and G. Iadonisi, Phys. Rev. B **66**, 113308 (2002).

[24] G. Cantele, F. Trani, D. Ninno, and G. Iadonisi, J. Phys.: Condens. Matter **15**, 5715 (2003).
[25] F. Trani, G. Cantele, D. Ninno, and G. Iadonisi, Physica E (Amsterdam) **22**, 808 (2004).
[26] F. Trani, G. Cantele, D. Ninno, and G. Iadonisi, Phys. Status Solidi C **2**, 3435 (2005).
[27] A. L. Efros and A. V. Rodina, Phys. Rev. B **47**, R10005 (1993).
[28] A. L. Efros, M. Rosen, M. Kuno, M. Nirmal, D. J. Norris, and M. Bawendi, Phys. Rev. B **54**, 4843 (1996).
[29] G. Allan, C. Delerue, and Y. M. Niquet, Phys. Rev. B **63**, 205301 (2001).
[30] D. Kovalev, B. Averboukh, M. Ben-Chorin, F. Koch, A. L. Efros, and M. Rosen, Phys. Rev. Lett. **77**, 2089 (1996).
[31] D. Kovalev, M. Ben-Chorin, J. Diener, F. Koch, A. L. Efros, M. Rosen, N. A. Gippius, and S. G. Tikhodeev, Appl. Phys. Lett. **67**, 1585 (1995).
[32] V. Y. Timoshenko, L. A. Osminkina, A. I. Efimova, L. A. Golovan, P. K. Kashkarov, D. Kovalev, N. Künzner, E. Gross, J. Diener, and F. Koch, Phys. Rev. B **67**, 113405 (2003).
[33] M. Cazzanelli, D. Kovalev, L. D. Negro, Z. Gaburro, and L. Pavesi, Phys. Rev. Lett. **93**, 207402 (2004).
[34] L. W. Wang and A. Zunger, Phys. Rev. Lett. **73**, 1039 (1994).
[35] L. Brey, C. Tejedor, and J. A. Vergés, Phys. Rev. B **29**, 6840 (1984).
[36] L. C. LewYanVoon and L. R. Ram-Mohan, Phys. Rev. B **47**, 15500 (1993).
[37] T. B. Boykin and P. Vogl, Phys. Rev. B **65**, 035202 (2002).
[38] B. A. Foreman, Phys. Rev. B **66**, 165212 (2002).
[39] T. G. Pedersen, K. Pedersen, and T. B. Kriestensen, Phys. Rev. B **63**, 201101(R) (2001).
[40] M. Cruz, M. R. Beltrán, C. Wang, J. Tagüeña-Martínez, and Y. G. Rubo, Phys. Rev. B **59**, 15381 (1999).
[41] J. R. Chelikowsky and M. L. Cohen, Phys. Rev. B **10**, 5095 (1974).
[42] D. E. Aspnes, *EMIS Datareviews series n 4* (INSPEC, The Institution of Electrical Engineers, London, 1988), pp. 70–79.
[43] G. Onida, L. Reining, and A. Rubio, Rev. Mod. Phys. **74**, 601 (2002).
[44] R. A. Faulkner, Phys. Rev. **184**, 713 (1969).
[45] D. L. Dexter, Solid State Phys. **6**, 353 (1958).
[46] C. Garcia, B. Garrido, P. Pellegrino, R. Ferre, J. A. Moreno, J. R. Morante, L. Pavesi, and M. Cazzanelli, Appl. Phys. Lett. **82**, 1595 (2003).
[47] R. Schäfer and J. A. Becker, Phys. Rev. B **54**, 10296 (1996).
[48] I. Vasiliev, S. Öğüt, and J. R. Chelikowsky, Phys. Rev. B **65**, 115416 (2002).
[49] M. Dovrat, Y. Goshen, J. Jedrzejewski, I. Balberg, and A. Sa'ar, Phys. Rev. B **69**, 155311 (2004).
[50] J. P. Wilcoxon, G. A. Samara, and P. N. Provencio, Phys. Rev. B **60**, 2704 (1999).
[51] M. S. Hybertsen, Phys. Rev. Lett. **72**, 1514 (1994).
[52] C. Delerue, G. Allan, and M. Lannoo, Phys. Rev. B **64**, 193402 (2001).
[53] C. Delerue, G. Allan, and M. Lannoo, Phys. Rev. B **48**, 11024 (1993).
[54] G. Allan, C. Delerue, M. Lannoo, and E. Martin, Phys. Rev. B **52**, 11982 (1995).
[55] F. Riboli, D. Navarro-Urrios, A. Chiasera, N. Daldosso, L. Pavesi, C. J. Oton, J. Heitmann, L. X. Yi, R. Scholz, and M. Zacharias, Appl. Phys. Lett. **85**, 1268 (2004).
[56] The symmetry group name in Ref. 25 contains a misprint. D_{2v} should be read as D_{2d}.
[57] This behavior is typical of the quantum confinement effect, also observed for the spherical nanocrystals. Indeed, the nanocrystal HOMO-LUMO gap energy reaches the bulk limit (with a precision of tens of meV) only for structures with diameter of several nanometers (Refs. 14 and 15), made of tens of thousands of silicon atoms.
[58] F. Buda, J. Kohanoff, and M. Parrinello, Phys. Rev. Lett. **69**, 1272 (1992).
[59] X. Zhao, C. M. Wei, L. Yang, and M. Y. Chou, Phys. Rev. Lett. **92**, 236805 (2004).
[60] D. D. D. Ma, C. S. Lee, F. C. K. Au, S. Y. Tong, and S. T. Lee, Science **299**, 1874 (2003).